sciendo

***MINERALOGIA**, 51,17-35 (2020)*
DOI: 10.2478/mipo-2020-0003
www.Mineralogia.pl

MINERALOGICAL SOCIETY OF POLAND
POLSKIE TOWARZYSTWO MINERALOGICZNE

Original paper

Analysis of selected mineral and waste sorbents for the capture of elemental mercury from exhaust gases

Magdalena Wdowin[1]*, Mariusz Macherzyński[2], Rafał Panek[3], Mateusz Wałęka[2], Jerzy Górecki[2]

[1] *Mineral and Energy Economy Research Institute, Polish Academy of Sciences, Wybickiego 7A, 31-261 Kraków, Poland*
[2] *AGH University Science and Technology, al. Mickiewicza 30, 30-059 Kraków, Poland3 Lublin University of Technology, Nadbystrzycka 40, 20-618 Lublin, Poland*
** Corresponding author*
e-mail: e-mail: wdowin@meeri.pl

Received: *October 12, 2019*
Received in revised form: *March 12, 2020*
Accepted: *July 6, 2020*
Available online: *November 5, 2020*

Abstract. Several mineralogically, chemically and texturally diverse minerals and waste materials were selected for the testing of elemental mercury capture in exhaust gas, namely tyre char resulting from the burning of pyrolytic rubber tyres, class C fly ash, mesoporous material type MCM-41 and glauconite. Each material's mineralogical, chemical and textural characteristics were explored. In order to conduct experiments in conditions similar to those during the contact of sorbent with real coal exhaust fumes at a temperature of about 110-120°C, the experiments were carried out using a test device consisting of a furnace for burning powdered coals, a thermostatic cage for sorbent reactors and mercury gas analysers, which are able to measure and compare the effects of individual sorbents with exhaust gas. The study found that the best results for mercury sorption in the exhaust atmosphere were obtained for class C ash resulting from brown coal combustion.

Key-words: mercury capture, exhaust gas, minerals, waste products

1. Introduction

The problem of mercury emissions from anthropogenic sources has become one of the main environmental issues in recent years. This element and its selected compounds are dangerous due to their high chemical and biological activity, toxicity, durability, and volatility, as well as the possibility of migration over long distances. By its release into the environment, mercury enters living organisms via food chains, where it accumulates to form many toxic compounds, both inorganic and organic. Because mercury has high bioaccumulation properties, its content in the biosphere of the Earth's crust is constantly increasing. According to the Agency for Toxic Substances and Disease Registry, mercury ranks third on the list of substances most hazardous to human health (Lavoie et al. 2013; Zhang et al. 2016).

In the new restrictions imposed by the IED (Industrial Emissions Directive) (Directive, 2010), the limits for mercury emissions from the energy sector are very strict.

For mercury emissions, standards are set at the following levels for hard coal:

- 1-3 $\mu g/Nm^3$ for new installations up to 300 MWt;
- 1-9 $\mu g/Nm^3$ for existing installations up to 300 MWt;
- 1-2 $\mu g/Nm^3$ for new installations above 300 MWt; and
- 1-4 $\mu g/Nm^3$ for existing installations with a capacity of over 300 MWt.

The standards for brown coal are as follows:

- 1-5 $\mu g/Nm^3$ for new installations up to 300 MWt;
- 1-10 $\mu g/Nm^3$ for existing installations up to 300 MWt;
- 1-4 $\mu g/Nm^3$ for new installations above 300 MWt; and
- 1-7 $\mu g/Nm^3$ for existing installations above 300 MWt.

In existing coal-based power plant solutions, the preliminary methods such as selective mining, composing coal mixtures, and enrichment of coal; primary methods including combustion in a fluidised bed and the use of low-emission NOx burners; and secondary methods involving the introduction of coal into the combustion chamber, and then removing mercury from the combustion gases generated in the combustion process (solid sorbent injection – mainly activated carbon), do not enable power plants to achieve the required emission limits; therefore, there is a need to search for new, effective solutions (Pacyna et al. 2008; Sloss 2008; Panasiuk et al. 2009; Wichliński et al. 2012).

A relatively easy solution that does not require costly investment is activated carbon injection technology (Powdered Active Carbons), involving the injection of a properly prepared sorbent into the flue gas after the boiler, but before the electrostatic precipitator. Mercury adsorbed on the sorbent is removed in the electrostatic precipitator, with the effectiveness of this method estimated to be up to 98% (Wichliński et al. 2012). The efficiency of the electrostatic precipitator in terms of mercury removal depends on (Bustard et al. 2004; Olson et al. 2009; Bujny et al. 2012):

- Mercury speciation in exhaust gases (Hg^{2+} adsorbs very well on the surface of sorbents, while Hg^0 practically is not adsorbed);
- Flue gas temperature (the higher the temperature, the lower the sorption effect);
- Flue gas composition, sorbent dose size (C: Hg atomic ratio), and the degree of sorbent mixing in the flue gas;
- The duration of sorbent contact with the flue gas; and
- The efficiency of dust removal devices.

This technology of activated carbon injection, however, has the following drawbacks: the effect on the sale or reuse of ash (Bustard et al. 2003); the injection of dusty sorbent may lead to clogging of the system; the solution is not suitable for wet exhaust gases or the sorbent in this case must be properly activated; there is a risk of self-ignition at temperatures higher than 120°C; and there is a risk of polymerisation of unsaturated hydrocarbons occurring in the flue gas draught on activated carbon (https://emis.vito.be).

In the combustion of fossil fuels (mainly lignite and hard coal), mercury is emitted in the form of gas, among others in the elemental form Hg^0, but also as divalent Hg^{2+} ions or solid particles, and mercury adsorbed on emitted dusts. The amount adsorbed on ash particles ranges from 5 to 10% of the total amount released during combustion processes. The other 90-95% is mercury in gaseous form. Elemental mercury Hg^0 is the most dangerous and durable form of mercury, which is associated with its long duration of stay in the atmosphere (from six months to two years) and transmission up to hundreds of kilometres from the source of emission (Galbreath, Zygarlicke 2000; Żmuda et al. 2017). Considering flue gas cleaning, the most difficult to capture is elemental mercury, as it is not removed by any of the conventionally applied flue gas cleaning systems and thus enters the atmosphere. From the thermodynamic calculations, it can be concluded that unfortunately the most stable form in the high temperature of the combustion processes is the elemental mercury Hg^0 in the gaseous phase, but oxidised forms are easy to capture (Grzywacz et al. 2015). Therefore, research into sorbents that oxidise mercury before capture is needed.

Many materials are the subject of research due to their oxidation, capture and catalysis potential for mercury. The most frequently studied include palladium, gold, iridium, platinum, iron, fly ash and activated carbons (Presto, Granite 2006; Wilcox et al. 2012).

Taking into consideration the lack of commercial mercury capture technologies on the market that meet the new BREF/BAT requirements, and since new technologies should be economically viable and relatively easy to implement on site, dry sorbent injection seems to be the most promising solution. The aim of this article is to analyse mineralogically, chemically and textural diverse solid sorbents in terms of their use as sorbents of gaseous forms of mercury from exhaust gases.

2. Samples and methods

2.1. Mineralogical analysis

X-ray phase analysis was performed through the powder method using a Panalytical X'Pert APD X-ray diffractometer (XRD) with a PW 3020 goniometer, a Cu lamp and a graphite monochromator. The analyses were performed in the angular range from 5 to 65 2θ. X'Pert software was used to process the diffraction data. The identification of mineral phases was based on the JCPDS-ICDD database.

For analysis using scanning electron microscopy (SEM), the FEI QUANTA 200 FEG microscope with EDAX's energy dispersion spectrometer (EDS) was used. Observations were carried out using secondary electrons.

Mineralogical studies enabled the characterisation of the structure (XRD, SEM), type (XRD, SEM) and the quantitative and qualitative mineral composition (XRD, SEM, Differential Thermal Analysis/Thermogravimetry) of the analysed fly ash and tyre char.

2.2. Chemical analysis

Determination of the elemental composition of both minerals as well as waste materials was carried out by the method of energy-dispersion X-ray fluorescence (XRF) using an Epsilon 3 spectrometer from Panalytical. The test was conducted in the Na-Am range on an apparatus equipped with an Rh 9W X-ray tube (50 kV, 1 mA), 4096 channel spectrum analyser, six measuring filters (Cu-500, Cu-300, Ti, Al-50, Al-200, Ag), and a high resolution solid state semiconductor (Silicon Drift Detector – SDD) detector (Be window, 50 um thick) cooled by Peltier cell. This study allowed the quantitative and qualitative share of individual elements to be to determined.

Because the XRF method enables the determination of the share of elements in the Na-Am range, carbon in the analysed material was determined by the infrared (IR) method after burning the sample in an oxygen atmosphere in an induction furnace (combustion induced by the addition of tungsten), where the resulting CO_2 was directed to the IR chamber and the absorption in the characteristic IR range was analysed for carbon. Then, the results of the XRF analyses were supplemented based on IR analysis of carbon.

2.3. Textural analysis

Texture tests were carried out using the Micromeritics ASAP 2020M sorptomate. The following parameters were determined: SBET - specific surface area (m^2/g), Vp - total pore volume (cm^3/g), Dp - average pore diameter (nm).

Textural properties such as the specific surface, specific surface of micropores, and measurement of the size and distribution of pores depending on the radius were determined on the basis of the course of nitrogen vapour adsorption/desorption at -194.85°C. The listed texture parameters of the tested materials were determined after earlier degassing the sample under strictly controlled temperature (250°C for 24 h) and reduced pressure (10^{-3} hPa). The specific surface was determined based on the theory of multilayer Braunauer-Emmett-Teller (BET) adsorption at p/p_0 between 0.06 and 0.3 (p, p_0 - equilibrium pressure and nitrogen saturated vapour pressure). The pore volume V_p was determined from the volume of adsorbed nitrogen at a pressure $p/p_0 = 0.98$. The pore diameters D_p were calculated according to the formula $D_p = 4V_p/SBET$. The pore volume distribution R_p was calculated from the general isotherm equation based on the combination of the modified Kelvin equation and the statistical thickness of the adsorbed film.

Textural analysis is one of the most important determinations in studying sorption processes. It enables the estimation of the specific surface, distribution and size of pores and their shape. These parameters are important for gas adsorption. The larger the specific surface, the better the sorption properties of the tested material. In contrast, the size and shape of the pores suggest what desorbed gas is able to enter into the structure of the sorbent being tested.

A large specific surface is responsible for facilitating contact of the adsorbed molecules with active centres located on the adsorbent surface, while the size and shape of the pores ensure proper transport of the adsorbate.

2.4. Tests of mercury removal from hard coal exhaust gases

Tests were performed in the experimental stand (described in detail by Macherzyński 2018). The coal used to produce flue gas was a Polish commercial low-rank hard coal for energy production that can be considered as sub-bituminous coal. Concentration of mercury in the coal was 95.7 ppb. The key equipment of the stand was as follows: flue gas generator, thermostatic fly ash filter, elemental mercury generator equipped with peristaltic pump (after the dust-filter the flue gas was enriched with elemental mercury at a level of about 20 $\mu g/m^3_N$), thermostatic cage for sorbent reactors and finally scrubbers that stabilised the flue gases before mercury analysis in two EMP-2 (NIC) elemental mercury (Hg^0) analysers. The exhaust gases content shown in Table 1 was obtained at a flow rate of 60l h^{-1}, while the generator was fed with several grams of hard coal powder per hour. The gas composition was measured by a Testo 350 Emission Analyzer.

TABLE 1

Parameters of flue gas used in the tests

Parameter	Unit	Value
λ	-	1.75
O_2	%	8.9-9.1
CO	ppm	60-62
CO_2	%	11.6-11.8
SO_2	ppm	585-665
H_2S	ppm	41-47
NO	ppm	306-311
NO_2	ppm	1.5-2

EMP-2 analysers can detect elemental mercury concentration in gas mixtures on-line with a quantification limit (QL) of 0.3 $\mu g/m^3_N$ at a resolution of 0.1 $\mu g/m^3_N$ by using the atomic absorption spectroscopy (AAS) method. The MA-3000 (NIC) can determine the total mercury (CHg_t) in solid and liquid samples by thermal decomposition, gold amalgamation, and the AAS determination method. It was used to compare the sorbents' effectiveness (capacities towards mercury during the tests). The thermostatic cage operates up to 180°C. Tests were performed in the 110-120°C range. In the case of char from used tyres, the test temperature range was 130-140°C. There were identical two glass reactors inside the cage: one was used as an empty reference trap while the other contained a 2 g fixed bed of tested sorbent. The same gas flow of 24l h^{-1} was regulated through both reactors. At this flow rate, the concentration of O_2 and CO_2 in the flue gas reached values similar to pc-fired boiler exhaust gases at around 5.5% and 15%, respectively, and λ ~1.35. By comparing the concentration of mercury in these two streams (cHgREF and cHgSORB), it is possible to calculate (1) the percent of mercury breakthrough ($Hg_{B\%}$) at a certain moment; (2) the total mercury load breakthrough ($Hg_{LB\%}$) after a specified time; and (3) the mean removal value ($Hg_{R\%}$) during 90 min when the exhaust gases are in contact with sorbents (the mean $1/Hg_{B\%}$). The following two formula were used to enable these calculations:

$$\mathrm{Hg}_{\mathrm{B\%}} = \left(1 - \frac{cHgSORB}{cHgREF}\right) \cdot 100\% \text{ (at the certain moment)} \tag{1}$$

$$\mathrm{Hg}_{\mathrm{LB\%}} \left(\frac{\sum mHgb\ behind\ SORB\ reactor}{\sum mHgb\ behind\ REF\ reactor}\right) \cdot 100\% = \text{(after a specified time)} \tag{2}$$

3. Results and discussion

3.1. Characteristics of tested sorbents

Several mineralogically, chemically and texturally diverse minerals and waste materials were selected for research:

1. Tyre char resulting from the pyrolytic combustion of rubber tyres at a temperature of 450^{o}C;
2. Class C fly ash resulting from the combustion of brown coal in a dust boiler;
3. Mesoporous material type MCM-41 obtained from waste products such fly ash, as well as reaction solution resulting from the synthesis of zeolite materials from fly ash; and
4. Glauconite, a mineral raw material obtained from Russian deposits.

Tyre char

Pyrolytic waste (tyre char) results from the burning of rubber tyres at a temperature of about 450°C. As a result of this process, recovered oils and dry pyrolysis waste are obtained, which were subjected to the tests in this study.

In the chemical composition of the tested waste, the dominant component is coal (78.8% by mass). The amounts of remaining ingredients expressed as oxides are as follows (% by mass): MgO 0.061; Al_2O_3 0.281; SiO_2 6.817; P_2O_5 0.053; SO_3 5.364; K_2O 0.098; CaO 1.287; TiO_2 0.023; Fe_2O_3 0.471; Co_3O_4 0.032; CuO 0.043; ZnO 3.879; Ag_2O 0.08; PbO 0.008.

The XRD diffraction pattern (Fig. 1) shows high background coming from carbon, as well as the presence of sulphur, calcite and quartz.

Observations of grain morphology (SEM-EDS; Fig. 2) showed the presence of carbon, with fine crystalline grains found in larger aggregates.

Textural analysis showed that, compared to high-carbon wastes, the tested waste has a low 73.72 m^2/g specific surface area. The average pore diameter is 14.64 nm, while the pore volume is 0.178 cm^3/g.

Hysteresis loops of adsorption/desorption isotherms (Fig. 3) indicate capillary condensation in the mesopores. The shape of the hysteresis loop suggests type III/IV according to the classification recommended by The International Union of Pure and Applied Chemistry's (IUPAC) characteristic for micro/mesoporous materials, which is associated with the presence of "bottle-shaped" pores, that is, "inkwell" and spherical pores with open ends and significant internal narrowing (Klinik 2000). However, the hysteresis shape according to the de Boer (1958) classification suggests type B, which according to the IUPAC classification corresponds to type H1, characteristic for bottle-shaped pores (narrow entrance to the wide interior), and also for pores formed between two planes with different mutual inclination.

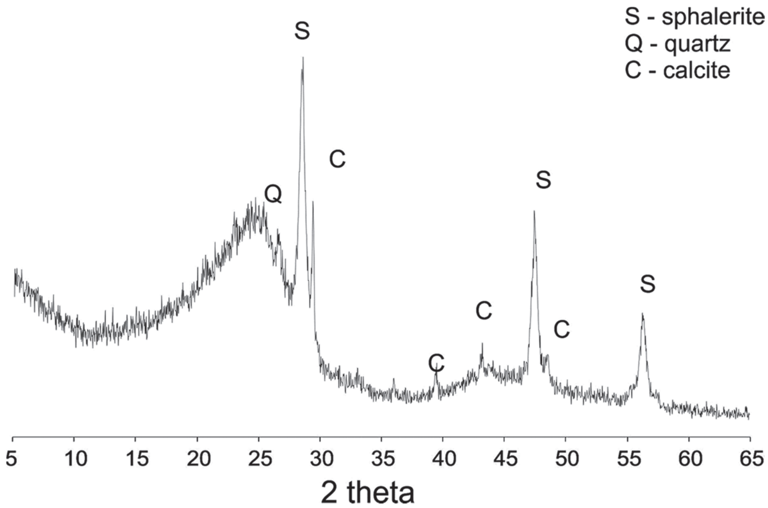

Fig. 1. XRD diffraction pattern of the mineral composition of the examined tyre char

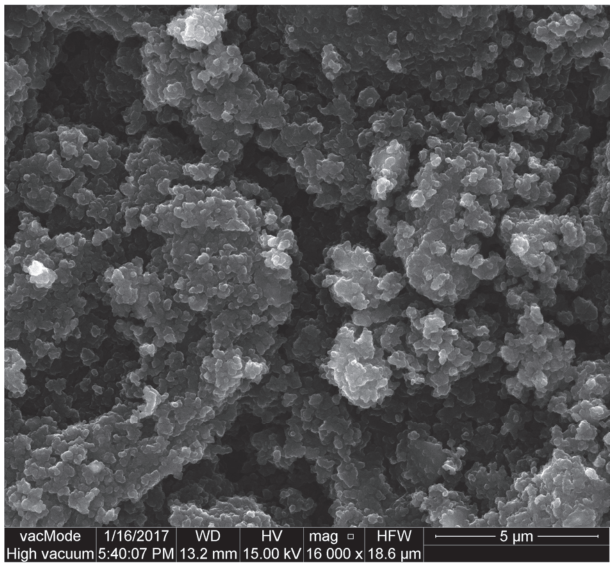

Fig. 2. SEM image of tyre char

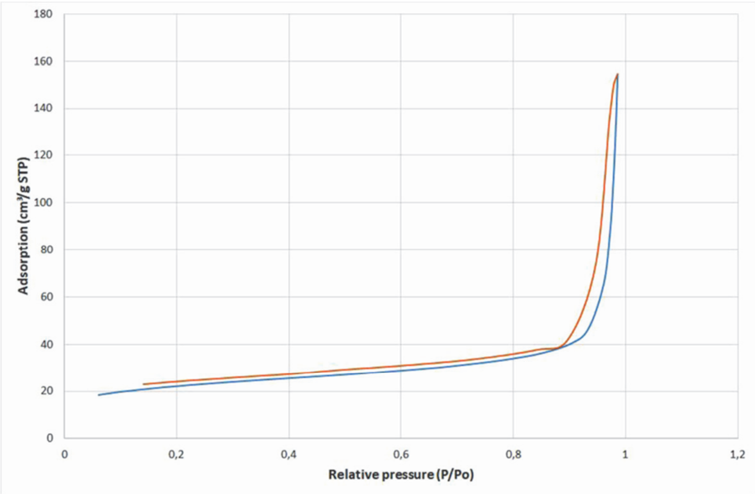

Fig. 3. N_2 adsorption / desorption isotherms for tyre char

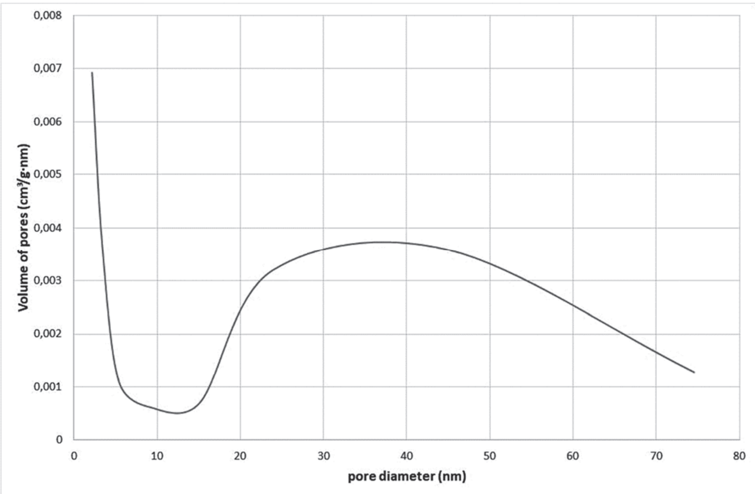

Fig. 4. Pore size distribution for tyre char

The pore size distribution of the examined carbonisate (Fig. 4) is homogeneous/modal and indicates a micro-/meso-porous character. A dominant share of pores with a diameter of 14 nm is observed (Czarna Juszkiewicz et al. 2018).

Fly ash C class

The dominant component in the chemical composition of the analysed ash is silicon (SiO_2 32.5% by mass) and calcium (CaO 25.7% by mass), as well as coal (19.0% by mass). The chemical composition of the other components expressed as oxides is as follows: MgO

2.935%; Al_2O_3 5.482%; P_2O_5 0.163%; SO_3 7.148%; K_2O 0.432%; TiO_2 1.102%; MnO 0.248%; Fe_2O_3 4.18%; NiO 44.5 ppm; CuO 37.7 ppm; Rb_2O 31.1 ppm; SrO; 0.152%; Y_2O_3 34.6 ppm; ZrO_2 0.042%; Ag_2O 0.102%; BaO 0.073%; PbO 78.4 ppm.

The XRD diffraction pattern (Fig. 5) of the mineral composition indicates the presence of quartz, anhydrite, gelenite and mullite. It is interesting that the spectrum has no background, which indicates the absence of an amorphous phase in the mineral composition of the studied fly ash.

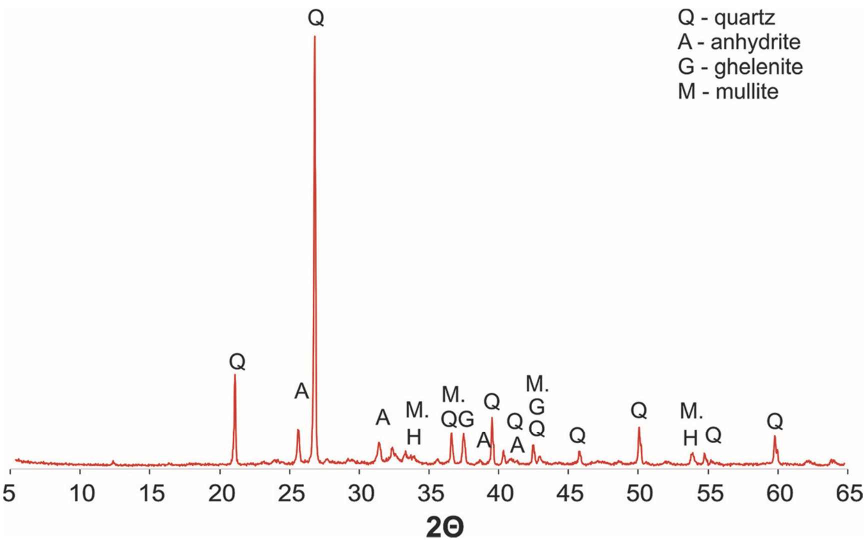

Fig. 5. XRD diffraction pattern of investigated fly ash

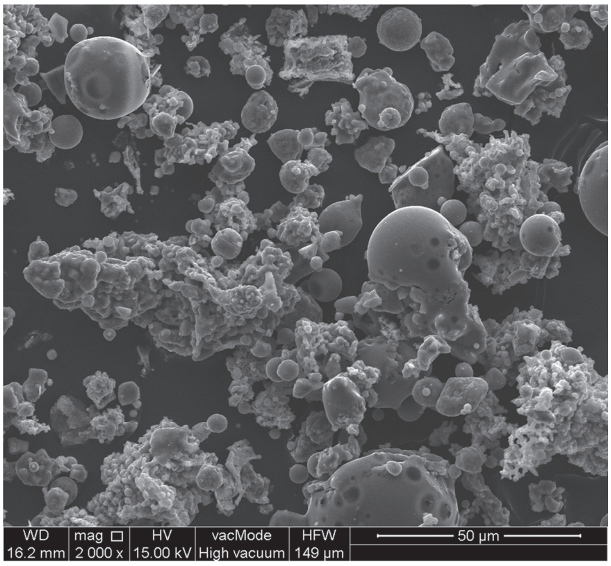

Fig. 6. SEM image of fly ash

Analysis of the grain morphology (Fig. 6) indicated the presence of both irregular and spherical grains as cenospheres and pleospheres with very different grain sizes.

In the textural analysis (Fig. 7, 8), a weak hysteresis loop and bimodal pore size distribution are visible.

The specific surface area was established at the level of 3.55 m^2/g, where the pore volume was 0.005 cm^3/g and the average pore diameter 6.9 nm.

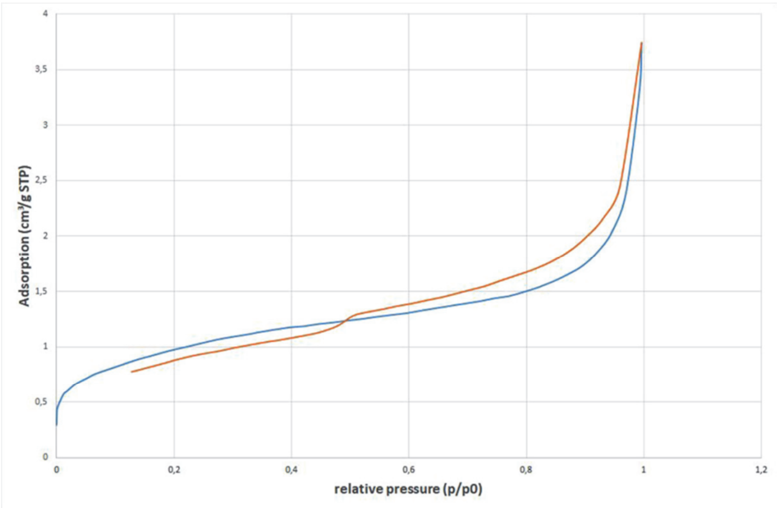

Fig. 7. N_2 adsorption/desorption isotherms for fly ash

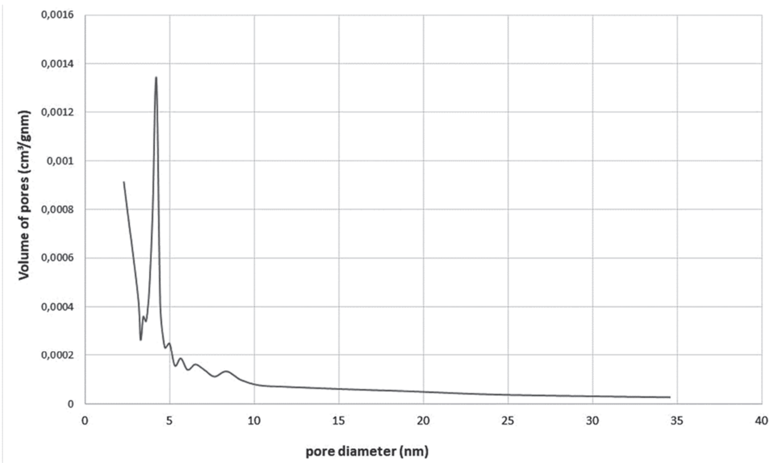

Fig. 8. Pore size distribution for fly ash

MCM-41

Material type MCM-41 was synthesised from a silica-rich by-product, namely filtrate obtained after the hydrothermal synthesis of zeolites (20 kg fly ash, 12 kg NaOH, 90 dm^3 H_2O, temperature 80°C, duration 36 h for the preparation of Na-P1 zeolite) using the installation described by Wdowin et al. (2014). Also, this material can be obtained from a waste solution rich in silica formed during the synthesis of other zeolites (Panek et al. 2017).

The chemical composition was as follows (in %): Na_2O 1.340; MgO 0.008; Al_2O_3 0.951; SiO_2 96.756; P_2O_5 0.439; SO_3 0.148; Cl 0.005; K_2O 0.010; CaO 0.120; TiO_2 0.026; V_2O5 0.033; Cr_2O3 0.001; MnO 0.002; Fe_2O_3 0.145; CuO 0.006; ZnO 0.009. Analysis indicated that the amount of MCM-41 is almost 97wt% as SiO_2. Insignificant amounts of Na_2O and Al_2O_3 are visible (about 1wt%). All other ingredients constitute less than 1wt%.

XRD diffraction pattern (Fig. 9) analysis showed that this material gives characteristic reflections in the low-angle range (i.e. 0-6 2 theta). The identification of MCM-41 material was based on the characteristic interplanar distances dhkl = 40.71, 23.56, 20.31, 15.26 Å.

Analysis of the grain morphology (Fig. 10) showed grain shapes close to spherical and partially elongated to 0.2 μm.

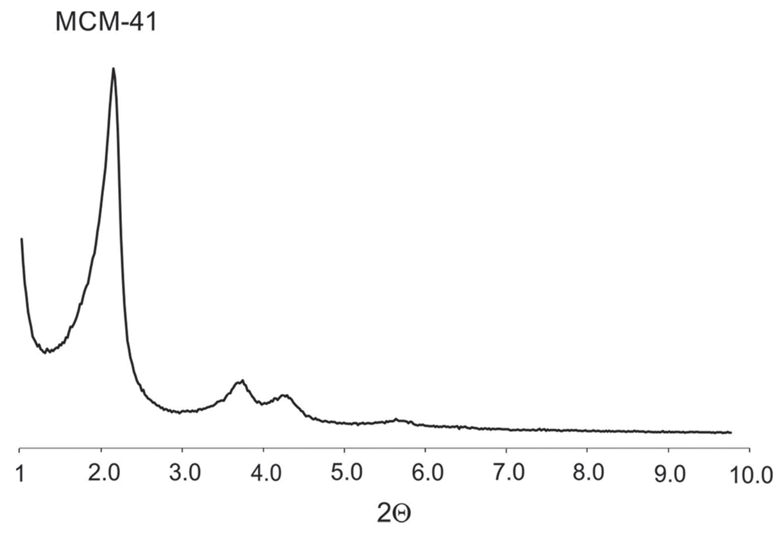

Fig. 9. XRD diffraction pattern of MCM-41

The N_2 sorption isotherms (Fig. 11) for MCM-41 are type IVB, which indicates a material with narrow mesopores. A sharp increase in the amount of adsorbed N_2 can be observed between 0.3 and 0.4 p/p_0, which is typical for this type of MCM-41 material. With detailed analysis in this area, a small hysteresis is observed, which is similar to H1 hysteresis (typical for commercial materials of this type (Panek et al. 2018)). It is important that MCM-41 has excellent pore homogeneity due to low hysteresis, which indicates the lack of pores about the inkwell.

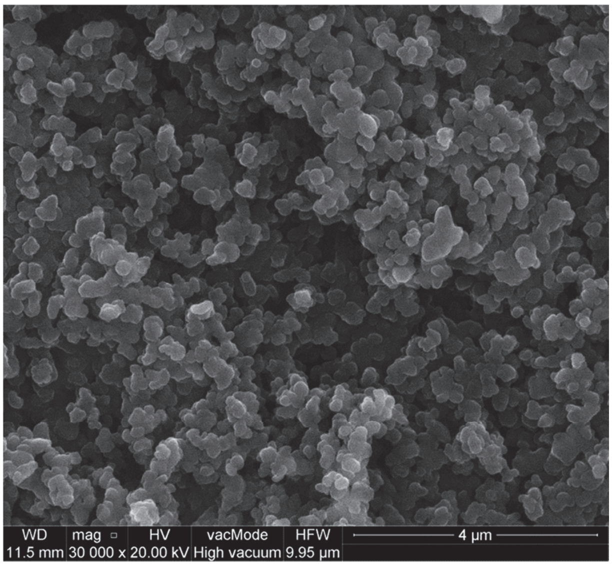

Fig. 10. SEM image of MCM-41

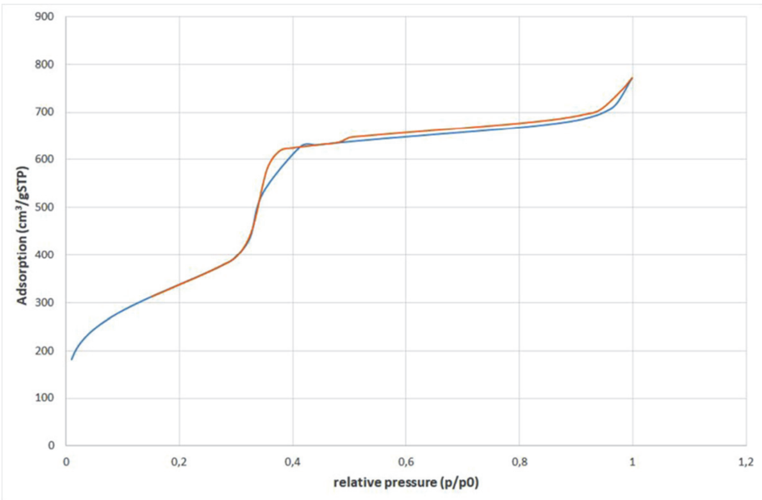

Fig. 11. N_2 adsorption/desorption isotherms for MCM-41

The distribution of pores (Fig. 12) is bimodal, with a predominant pore diameter of 2 and 4 nm.

The BET specific surface area was established at the level of 1222.69 m^2/g, pore volume 1.30 cm^3/g, and mean pore diameter 2.1 nm.

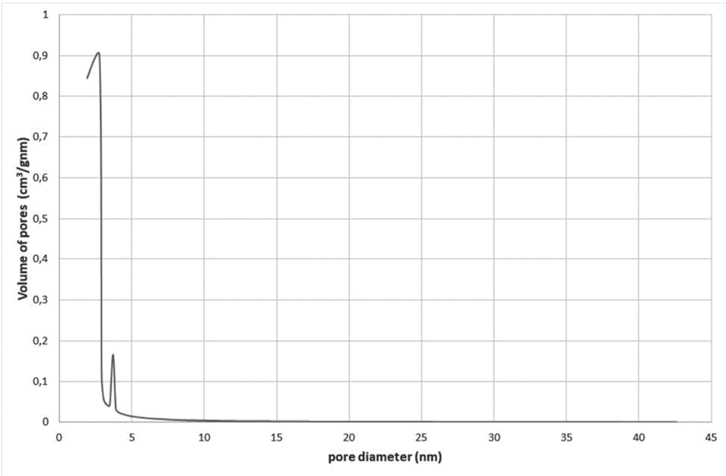

Fig. 12. Pore size distribution for MCM-41

Glauconite

The chemical composition shows the dominance of silica (SiO_2 64.565) and iron (Fe_2O_3 17.959). The other elements converted to oxides are as follows: MgO 2.771%; Al_2O_3 7.422%; P_2O_5 0.379%; K_2O 5.055%; CaO 1.167%; TiO_2 0.375%; Cr_2O_3 0.087%; MnO 0.032%; ZnO 0.011%; Rb_2O 0.03%; SrO 0.013%; Y_2O_3 73.9 ppm; ZrO_2 0.012%; Ag_2O 0.11%; PbO 43.6 ppm.

The mineral composition (Fig. 13) is dominated by glauconite and quartz, and small amounts of feldspars.

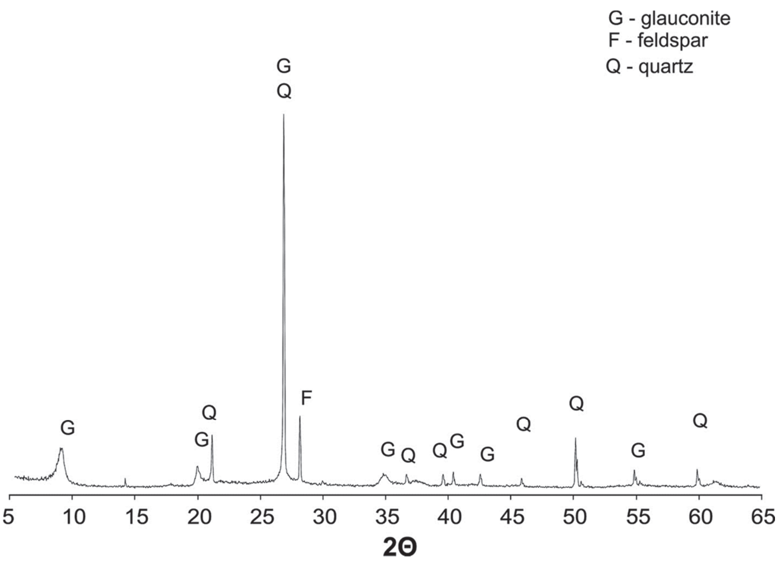

Fig. 13. XRD diffraction pattern of glauconite

The identification of glauconite was based on the characteristic interplanar distances dhkl = 10.1Å, 4.53Å, 3.63Å, 3.33Å, 3.09Å, 2.59Å, 2.40Å, 1.511Å.

Observations via SEM-EDS (Fig. 14) showed the presence of layered glauconite aggregates. In places, grains of quartz are visible.

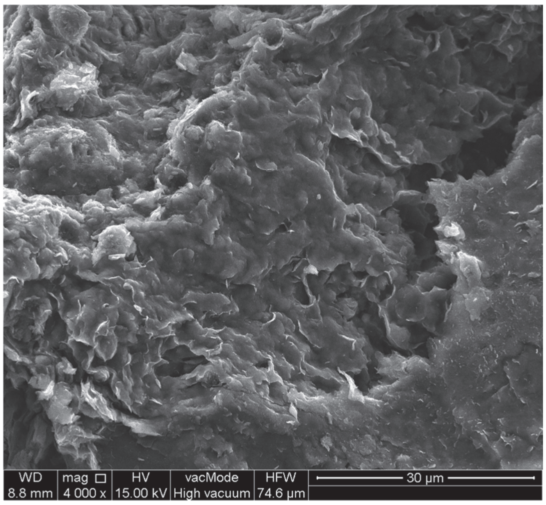

Fig. 14. SEM image of galuconite

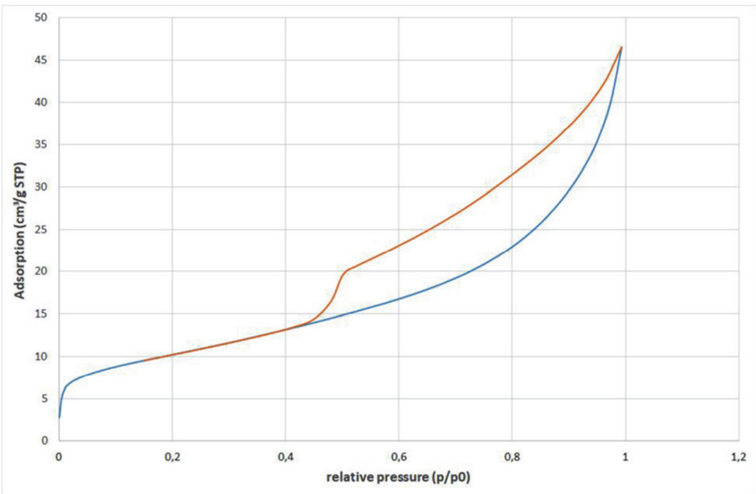

Fig. 15. N2 adsorption/desorption isotherms for glauconite

Textural investigation (Fig. 15, 16) showed that glauconite has a BET specific surface area of 36.77 $m^2 \cdot g^{-1}$. Its nitrogen adsorption–desorption isotherm shape can be classified as IV type (with hysteresis loop) according to the IUPAC classification, which is associated with capillary condensation in mesopores. The shape of the hysteresis established by de

Boer (1958) indicates type B, which is related to the presence of bottle-shaped pores. The hysteresis loop is close to the H3 type in the IUPAC classification, which is characteristic for mesopores in the shape of narrow slits. Textural analyses showed a modal pore distribution with a predominant pore size of 4 nm. The pore volume was evaluated at the level of 0.08 cm^3/g with an average pore size of 6.3 nm.

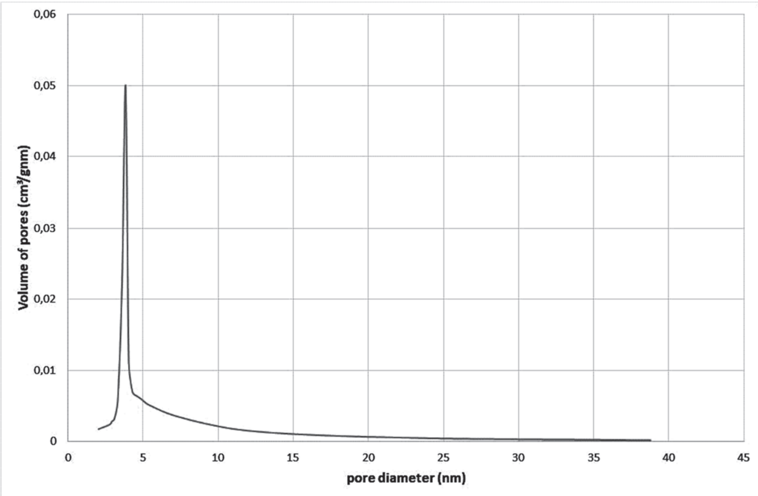

Fig. 16. Pore size distribution for glauconite

3.2. Results of the material tests in flue gas

The experiments of mercury capture consisted of several steps:

1. Zero base-line stabilisation;
2. Mercury (Hg^0) feeding from a generator (stabilisation of the reference mercury concentration);
3. Flue gas generation and contact with a fixed bed (90 min); and
4. Flue gas and mercury feeding exclusion.

In Figure 17 and Figure 18, the mercury capture is expressed as $Hg_{B\%}$. The fly ash shows a higher values of this parameter in the hot air fed by Hg^0 (> 50%) than in flue gas (about 25%). After switching off the exhaust gas at the end of the test, $Hg_{B\%}$ began to increase again. The char from used tyres, despite containing almost 79% carbon, has a higher $Hg_{B\%}$ of 53-54%. In the case of the fly ash, the presence of flue gas components has a clear effect on mercury capture. It can be assumed that part of the elemental mercury passes into the oxidised form, which easily adsorbs on ash grains, or that the exhaust components catalyse the heterogeneous reaction of mercury oxidation on the surface of the ash and the transition of mercury from the gas phase to the sorbent. In contrast, the tyre char was highly stable during the tests, but no significant difference was observed in the $Hg_{B\%}$ coefficient between air or flue gas enriched with elemental mercury. Its relatively low efficiency can be associated, among others, with small grain size, because this type of powder with an average grain size less than 20 μm forms a closed system with a compact consistency and flowing exhaust gases create privileged channels (no contact of all sorbent with flue gas is assumed). In contrast, the fly ash bed with higher particle size is more permeable to flue gas in its entire volume (Wdowin et al. 2015). After disconnecting the source of elemental mercury, both tests showed a rapid decrease in the concentration of this element in the gas passing through the beds of sorbents, despite maintaining a high measurement temperature. This indicates the stable capture of mercury by both sorbents. The waves appearing on the charts are associated with the sinusoid of the operating temperature of the entire measuring system. It tends to release small amounts of mercury outside the sorbent bed at higher temperatures. The measuring line with the reference reactor does not show sinusoidal mercury concentration waveforms if it is properly heated and clean. It is much more difficult to achieve such a state in a measuring line with a reactor filled with sorbents, because of Teflon tubes' "memory" coming from dirt and dustiness (Macherzyński 2018).

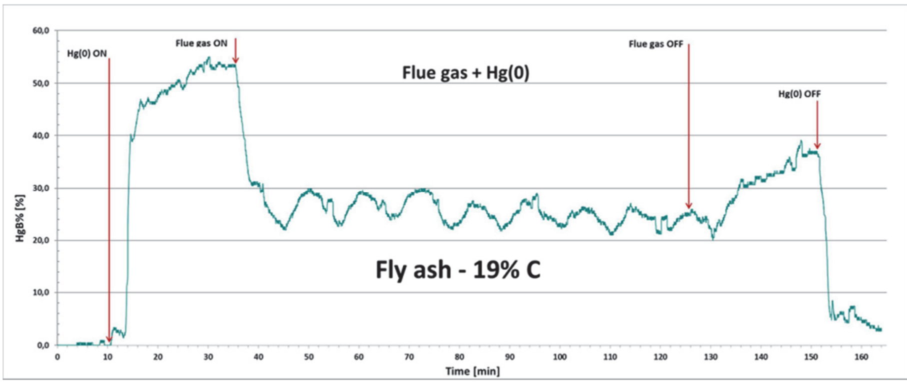

Fig. 17. Percent of mercury breakthrough (HgB%) in a fly ash fixed bed being in contact with flue gas

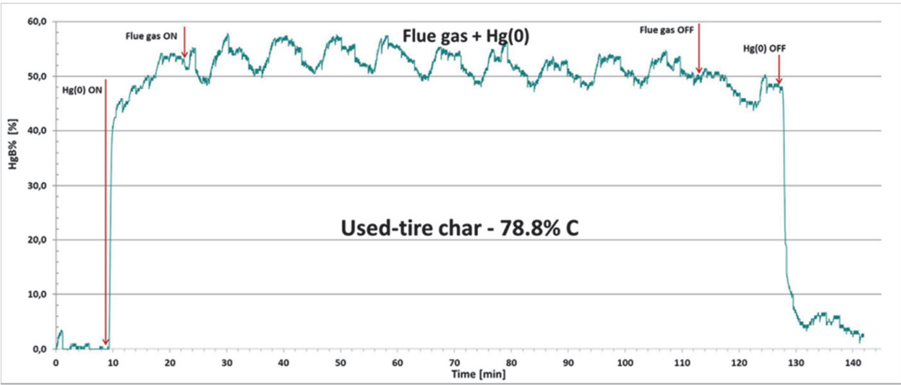

Fig. 18. Percent of mercury breakthrough (HgB%) in a used-tire char fixed bed being in contact with flue gas

Unlike the waste tyre char and high carbon content fly ash, mesoporous silica material (MCM-41) with a very large specific surface did not retain significant amounts of mercury from the exhaust gases (Fig. 19). It was highly permeable up to 100% of Hg^0 from the warm air stream. When the flue gas was turned on, the material underwent some activation but did not improve beyond approximately 80% of $Hg_{B\%}$. However, after turning off the flue gas, the sorbent showed mercury adsorption properties to some extent, so that $Hg_{B\%}$ dropped temporarily to 20-30%. After disconnecting the Hg^0 source, the material showed a tendency to release some of the elemental mercury caught in the test, which indicates mercury reemission from its grains. The total mercury concentration in the sorbent after the test was 85.2 ppb, which is low in relation to the potential and measured mercury sorption of the previously discussed carbon-containing materials (Table 2). The same situation applies to the granulated glauconite, in which the mercury concentration after the sorption test only increased from 1.6 ppb to an average of 18 ppb, and this material did not show measurable sorption properties in relation to the elemental mercury in the exhaust gases.

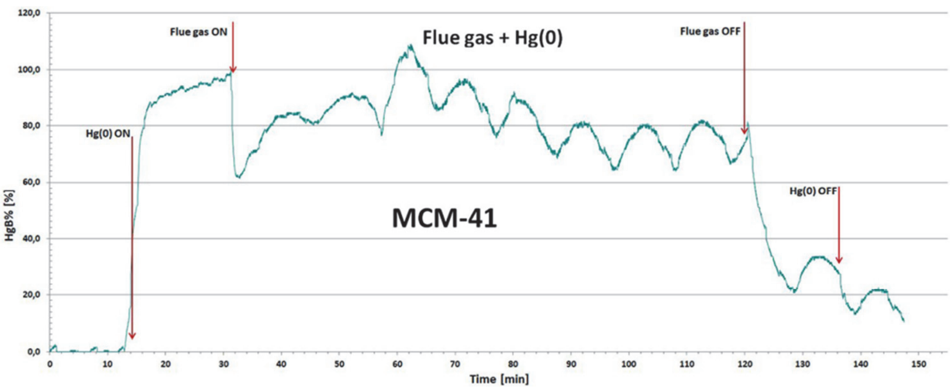

Fig. 19. Percent of mercury breakthrough (HgB%) in an MCM-41 fixed bed being in contact with flue gas

TABLE 2

Comparative parameters determining the suitability of sorbents for mercury capture from pc-powdered boiler exhaust gases

Sorbent	Load of mercury [μg]	CHg_t before test [ppb]	CHg_t after test [ppb]	$Hg_{LB\%}$ aftet stabilization [%]	Stabilization time [minutes]	$Hg_{R\%}$ [%]
Fly ash	1.20	82.5	616.8	27-30	25	82.0
Tire char	0.93	0.1	284.0	45-47	60	46.4
MCM-41	0.79	2.2	85.2	70-72	65	18.7
Glauconite	0.62	1.6	18.0	*	-	<5

* difficult to measure, unstable and often exceeding 100%

A summary of the parameters that determine the suitability of a given sorbent for mercury retention under test conditions is presented in Table 2. Comparison of the total mercury concentrations (CHg_t) before and after the test allows the assessment of the sorption potential of each material, especially in the context of the mass of elemental mercury that flowed through the bed during the entire test (see column two). The total mercury load breakthrough ($Hg_{LB\%}$) should be as low and stable as possible. Fly ash definitely stands out in this parameter, showing satisfactory mercury capture and potential for further industrial tests. This is confirmed by the last parameter: the mean removal value ($Hg_{R\%}$) during 90 min of each test ($Hg_{R\%}$).

4. Conclusion

We investigated potential sorbents differentiated mineralogically, chemically and texturally, in terms of capturing the elemental mercury from exhaust gases in identical conditions, that is, the same exhaust gas composition and flow rate of 24l h^{-1}.

The most important parameter in mercury capture for the tested materials was not the BET surface area as well as the particle size and pore volume, where in the case of materials such as MCM-41 this parameter was very good for consideration as a sorbent (BET surface area above 1200 m^2/g), but that material had the lowest value for mercury capture. While the chemical composition (high content of carbon) plays an important role, the affinity and probable structure of unburned coal residue is crucial. Therefore, fly ash C class gave the most promising result, where the capture of Hg(0) was at the level of 80%. A lower value was obtained for the tyre char (above 45%). The two others tested materials (i.e. MCM-41 and glauconite) gave poor results below 18%. Therefore, while its utilisation is limited, after proper development and stabilisation fly ash C class could be a new and cost-effective dedicated mercury sorbent.

Based on the obtained results, we can conclude that the sorption processes of elemental mercury should be investigated in detail, with suitable recognition of the chemical affinity or magnetic nature, as well as other factors that influence the efficiency of mercury sorption. Therefore, the next step will be research into the sorption nature, as well as the detailed examination of mercury sorption for the case of fly ash C class as the cheapest (by creating a circular economy) solution for mercury capture technology.

Acknowledgement. This work was financed by the National Centre for Research and Development project (Lider contract number LIDER/384/L-6/14/NCBR/2015) as well as the statutory work of Mineral and Energy Economy Research Institute, Polish Academy of Sciences.

5. References

Bujny, M., Burmistrz, P., Gruszka, S., Janicki, W., Kogutt, K., & Strugała, A. (2012). Instalacja demonstracyjna do monitorowania i redukcji emisji rtęci ze spalania węgla kamiennego w kotłach pyłowych. *Polityka Energetyczna, 15*(4), 161-174.

Bustard, J., Durham, M., Lindsey, C., Starns, T., Martin, C., Schlager, R., Sjostrom, S., Renninger, S., McMahon, T., Monroe, L., Goodman, J. M,. & Miller, R. (2003). Results of Activated Carbon Injection for Mercury

Control Upstream of a COHPAC Fabric Filter. The Mega Meeting: Power Plant Air Pollution Control Symposium, Washington D.C., May 19-22.

Bustard, J., Durham, M., Starns ,T., Lindsey, Ch., Martin, C., Schlager, R., & Baldrey K. (2004). Full-scale Evaluation of Sorbent Injection for Mercury Control on Coal-fired Power Plants. *Fuel Processing Technology, 85*(6-7), 549-562. DOI: 10.1016/j.fuproc.2003.11.021.

Czarna-Juszkiewicz, D., Wdowin, M., Kunecki, P., Baran, P., Panek, R., & Żmuda, R. (2018). Charakterystyka odpadu po pirolizie opon oraz analiza jego potencjalnego wykorzystania. Zeszyty Naukowe Instytutu Gospodarki Surowcami Mineralnymi Polskiej Akademii Nauk 107, 19-32.

Dyrektywa Parlamentu Europejskiego i Rady 2010/75/UE z dnia 24 listopada 2010 r. w sprawie emisji przemysłowych (zintegrowane zapobieganie zanieczyszczeniom i ich kontrola).

Galbreath, K.C., & Zygarlicke, Ch.J. (2000). Mercury Transformation in Coal Combustion Flue Gas. *Fuel Processing Technology*, *65-66*, 289-310. DOI: 10.1016/S0378-3820(99)00102-2.

Grzywacz, P., Dziok, T., & Porada, S. (2015). Behavior of Mercury in the Processes of Energo-Chemical Coal Processing in. Mercury As a Coal Combustion Pollutant [eds.] Gołaś J., Strugała A., Published and printed by Oficyna Drukarska – Jacek Chmielewski. pp. 152.

https://emis.vito.be

Lavoie, R., Jardine, T. D., Chumchal, M. M., Kidd, K., & Campbell, L. M. (2013). Biomagnification of Mercury in Aquatic Food Webs: A Worldwide Meta-Analysis. *Environmental Science & Technology, 47*, 13385-13394. DOI: 10.1021/es403103t.

Macherzyński, M. (2018). Redukcja emisji rtęci do środowiska – wybrane problemy w świetle badań laboratoryjnych i przemysłowych. Wydawnictwa AGH, seria Rozprawy - monografie nr 330, Kraków 2018.

Olson, E. S., Azenkeng, A., Laumb, J. D., Jensen, R. R., Benson, S. A., & Hoffmann, M. R. (2009). New Developments in the Theory and Modeling of Mercury Oxidation and Binding on Activated Carbons in Flue Gas. *Fuel Processing Technology, 90*(11), 1360-1363. DOI: 10.1016/j.fuproc.2009.08.006.

Pacyna, J. M., Sundseth, K., Pacyna, E. G., Munthe, J., Belhaj, M., Astrom, S., Panasiuk, D., & Głodek, A. (2008). Socio-economic costs of continuing the status-quo of mercury pollution, GLOCBA-SE Report, Nordic Council of Ministers, TemaNord 2008:580, Copenhagen, http://www.norden.org/no/publikasjoner/publikasjoner/2008-580.

Panasiuk, D., Pacyna, J. M., Głodek, A., Pacyna, E. G., Sebesta, L., &Rutkowski, T. (2009). Szacowanie kosztów zanieczyszczenia rtęcią dla scenariusza status-quo, raport MERCPOL etap I, Katowice.

Panek, R., Wdowin, M., Franus, W., Czarna, D., Stevens, L. A., Deng, H., Liu, J., Sun, C., Liu, H., C Snape C.E. (2017). Fly ash-derived MCM-41 as a low-cost silica support for polyethyleneimine in post-combustion CO2 capture. *Journal of CO_2 Utilization,* 22, 81-90. DOI: 10.1016/j.jcou.2017.09.015.

Presto, A. A., Granite, E. J. (2006). Survey of catalysts for oxidation of mercury in flue gas. *Environmental Science & Technology, 40*(18), 5601-5609. DOI: 10.1021/es060504i.

Sloss, L. (2008). Economics of mercury control. CCC/134, s.60.

Wdowin, M., Macherzyński, M., Panek, R., Górecki, J., & Franus, W. (2015). Investigation of the sorption of mercury vapour from exhaust gas by an Ag−X zeolite. *Clay Minerals, 50,* 31-40. DOI: 10.1180/claymin.2015.050.1.04.

Wichliński, M., Kobyłecki, R., & Bis, Z. (2012). Przegląd metod ograniczenia emisji rtęci w elektrowniach podczas spalania paliw stałych. *Polityka Energetyczna* 15(4), 151-160.

Wilcox, J., Rupp, E., Ying, S.C., Lim, D.H., Negreira, A.S., Kirchofer, A., Feng, F., & Lee, K. (2012). Mercury adsorption and oxidation in coal combustion and gasification processes. *International Journal of Coal Geology, 90*, 4-20. DOI: 10.1016/j.coal.2011.12.003.

Zhang, L., Wang, S., Wu, Q., Wang, F., Lin, C. J., Zhang, L., Hui, M., Yang, M., Su, H., & Hao, J. (2016). Mercury transformation and speciation in flue gases from anthropogenic emission sources: A critical review. *Atmospheric Chemistry and Physics. 16*, 2417–2433. DOI: 10.5194/acp-16-2417-2016.

Żmuda, R., Adamczyk, W., Lelek, Ł., Mandrela, S., Wdowin, M. (2017). Innowacyjna technologia oczyszczania spalin z rtęci jako rozwiązanie sprostania wymogom stawianym przez konkluzje BAT/BREF w polskiej energetyce. *Polityka Energetyczna - Energy Policy Journal 20*(4), 103-116.